Biomaterials 34 (2013) 508–515

Contents lists available at SciVerse ScienceDirect

Biomaterials

journal homepage: www.elsevier.com/locate/biomaterials

Long-term *in vivo* biodistribution and toxicity of $Gd(OH)_3$ nanorods

Yang Yang [a], Yun Sun [a], Ying Liu [a], Juanjuan Peng [a], Yongquan Wu [a], Yingjian Zhang [b], Wei Feng [a,*], Fuyou Li [a,*]

[a] Department of Chemistry & Institute of Biomedical Science, Fudan University, 220 Handan Road, Shanghai 200433, PR China
[b] Cancer Hospital, Fudan University, 270 Dongan Road, Shanghai 200032, PR China

ARTICLE INFO

Article history:
Received 11 September 2012
Accepted 29 September 2012
Available online 23 October 2012

Keywords:
$Gd(OH)_3$
Nanorods
Long-term toxicity
Biodistribution
Single photon emission computed tomography (SPECT)

ABSTRACT

The long-term retention of nanomaterials in the body is one of the biggest concerns about the safety of these materials for *in vivo* application. So, it is important to develop some nanomaterials which can be relatively more easily excreted. Rare earth hydroxide, that can be degraded under acidic condition *in vivo*, is one of the suitable candidates. Herein, $Gd(OH)_3$ nanorods, which are considered as magnetic resonance imaging (MRI) contrast agents, have been synthesized to evaluate their excretion process and potential toxicity. The long-term *in vivo* biodistribution of the materials was investigated using single photon emission computed tomography (SPECT) imaging with ^{153}Sm-doped $Gd(OH)_3$ nanorods as probes. Biodistribution results showed that the uptake and retention of the $Gd(OH)_3$ nanorods took place primarily in the liver, spleen and lung. Then, most of the nanorods were excreted from the bodies of mice very rapidly. Body weight data for the mice indicated that, when intravenously injected with 100 mg/kg of the nanorods, the mice survived for 150 days without any apparent adverse effects to their health. In addition, histological, hematological and biochemical analysis indicated that these nanorods have no overt toxicity.

1. Introduction

Due to their unique 4f electron structure, lanthanide-based nanomaterials exhibit rich optical and magnetic properties, and have attracted increasing attention in biomedical applications [1–8]. For example, under continuous-wave (CW) excitation at 980 nm, lanthanide nanoparticles co-doped with Yb^{3+} and Er^{3+} (or Tm^{3+}) show special upconversion luminescence (UCL) with unique properties, such as sharp emission lines, large anti-Stokes shifts of several hundred nanometers, superior photostability, and non-blinking [9–15]. Using such upconversion nanoparticles (UCNPs) as probes, high-contrast imaging of living cells and whole-body imaging of small animals have been achieved [16–24]. Combined with magnetic or other optical properties from lanthanide ions, multifunctional lanthanide nanoparticles have also been applied in multimodal bioimaging [25–34].

Nevertheless, there remain many unresolved issues regarding how lanthanide nanomaterials interact with biological systems. To date, there have been only a few studies concerning the *in vivo* biodistributions of rare earth nanomaterials and their long-term toxicities. Zhang et al. demonstrated the biodistribution of core–shell structured silica/$NaYF_4$ nanocrystals in a rat model [35]. Liu et al. reported *in vivo* pharmacokinetics, biodistribution, and toxicology of polymer-coated upconversion nanoparticles (UCNPs) in mice [36]. Recently, our group reported *in vivo* biodistribution and toxicity after 115 days using polyacrylic acid (PAA)-coated $NaYF_4$ UCNPs, and found that most of the PAA-UCNPs in the liver and spleen were cleared from the bodies of mice slowly and without any evident toxic effects [37]. These observations were all focused on $NaYF_4$-based UCNPs and the analysis techniques were based on the ICP-MS analysis of rare-earth ions in organs. In addition, the above results all indicated the metabolic and excretion processes involving nanomaterials in the body were slow. Because the usual long-term retention of nanomaterials in the body was one of the biggest concerns about the safety of the nanomaterials for *in vivo* use, it is important to develop some nanomaterials that are more easily degraded and more quickly excreted *in vivo*.

Due to its seven unpaired electrons, Gd^{3+} has excellent magnetic properties. Recently, $Gd(OH)_3$ nanorods have been reported to be a good magnetic resonance imaging (MRI) contrast agent [38]. Meanwhile, the rare earth hydroxides can be degraded under the acidic conditions such as exist in the lysosomes. So, the

* Corresponding authors. Department of Chemistry & Advanced Materials Laboratory, Fudan University, 220 Handan Road, Shanghai 200433, PR China. Fax: +86 21 6564 3270.
E-mail addresses: fengweifd@fudan.edu.cn (W. Feng), fyli@fudan.edu.cn (F.Y. Li).

0142-9612/$ – see front matter © 2012 Elsevier Ltd. All rights reserved.
http://dx.doi.org/10.1016/j.biomaterials.2012.09.075

$Gd(OH)_3$ nanorods were believed, at least potentially, to be easily excreted MRI agents. However, no studies concerned long-term toxicity, *in vivo* biodistribution imaging or *in vivo* sequestration and excretion of these one-dimensional nanorods. The main reason is the lack of effective imaging technique to track the materials with high sensitivity. Single photon emission computed tomography (SPECT) is an attractive method that allows three-dimensional localization of gamma emitters using a noninvasive procedure under *in vivo* conditions. For SPECT imaging, radioactivity signals can easily quantify the biodistribution of the radioactive element labeled materials *in vivo*, due to their high sensitivity and tissue penetration depth [39–47]. ^{153}Sm (E_γ = 103 keV) emits both medium-energy beta particles and a gamma photon, with a physical half-life of 46.3 h (1.93 days), which is long enough to be propitious to research about the long-term distribution of $^{153}Sm^{3+}$ labeled materials. In the present study, $Gd(OH)_3$ nanorods were synthesized and their biodistribution *in vivo* and long-term toxicity were investigated. Our strategy to dope the $Gd(OH)_3$ crystal lattices with radioactive $^{153}Sm^{3+}$ enabled us to investigate the *in vivo* biodistribution and metabolism of the $Gd(OH)_3$ nanorods by SPECT imaging and γ-counter mearsurements. Other toxicity assessments, such as body weight fluctuation, histological, hematological and biochemical analysis are also carried up to evaluate the long-term toxicity of $Gd(OH)_3$ nanorods.

2. Experimental section

2.1. Materials

Rare earth oxides Gd_2O_3 (99.999%) were purchased from Shanghai Yuelong New Materials Co. Ltd. Triethylamine (TEA), ethanol and hydrochloric acid were purchased from Sinopharm Chemical Reagent Co., China. Deionized water was used throughout. Rare earth chloride stock solutions were prepared by dissolving the corresponding metal oxide in hydrochloric acid at elevated temperature. Aqueous solution of $^{153}SmCl_3$ was purchase from HTA Co., Ltd., China.

2.2. Synthesis of gadolinium hydroxide nanorods

In a typical synthesis, 1 mmol of $GdCl_3$ was put into a Teflon-lined autoclave of 50 mL capacity and dissolved in 20 mL deionized water under stirring at room temperature. And then 3 mL of triethylamine (TEA) was added dropwise in the solution. The autoclave was filled with deionized water up to 80% of the total volume; after 15 min of stirring, it was sealed and maintained at 160 °C for 8 h without shaking or stirring. The autoclave was allowed to cool down to room temperature naturally. The precipitates were separated by centrifugation, washed with deionized water and absolute ethanol, and finally dried in air at the room temperature.

2.3. Synthesis of ^{153}Sm doped gadolinium hydroxide nanorods

In a typical synthesis, 0.1 mmol of $GdCl_3$ and 0.1 mL aqueous solution of $^{153}SmCl_3$ (~40 mCi) was put into a Teflon-lined autoclave of 5 mL capacity and dissolved in 2 mL deionized water under stirring at room temperature. After that 0.3 mL of TEA solution was added dropwise in the solution. The autoclave was filled with deionized water up to 80% of the total volume; after 15 min of stirring, it was sealed and maintained at 160 °C for 8 h without shaking or stirring. The system was allowed to cool naturally to room temperature, and the products were separated by centrifugation. The upper solution has no radioactivity signals which means all of the Sm^{3+} were incorporated into the $Gd(OH)_3$ nanocrystals. The resulting products ^{153}Sm doped $Gd(OH)_3$ nanorods were washed with deionized water and absolute ethanol, and finally dried in air at the room temperature. For further TEM characterization experiments, the ^{153}Sm-doped $Gd(OH)_3$ nanorods were stored at least 20 days, until the radioactivity left could not be detected by the radioactivity meter.

2.4. Characterization

X-ray powder diffraction (XRD) measurements of the $Gd(OH)_3$ nanorods were performed on a Bruker D4 diffractometer at a scanning rate of 1° min^{-1} in the 2θ range of 10–80°, with graphite monochromated Cu Kα radiation (λ = 1.5406 nm). The size and morphology of the nanocrystals were determined with a JEOL JEM-2010 transmission electron microscope (TEM) operated at 200 kV. Fourier transform infrared (FTIR) spectra were obtained on an IRPRESTIGE-21 spectros\lkjhngbcope (Shimadzu) with KBr pellets.

2.5. Cytotoxicity assay

The *in vitro* cytotoxicity was measured using 3-(4,5-dimethylthiazol-2-yl)-2,5-diphenyltetrazolium bromide (MTT) assay. A human nasopharyngeal epidermal carcinoma cell line (KB cell) was provided by Shanghai Institutes for Biological Sciences (SIBS), Chinese Academy of Sciences (CAS, China). KB cells growing in log phase were seeded into a 96-well cell-culture plate at 5×10^4/well and then incubated for 24 h at 37 °C under 5% CO_2. RPMI 1640 (Roswell Park Memorial Institute's medium) solutions of $Gd(OH)_3$ nanorods (100 μL/well) at concentrations of 200, 400, 600, 800, 1000 μg/mL were added to the wells of the treatment group, and RPMI 1640 (100 μL/well) to the negative control group, respectively. The cells were incubated for 24 h and 48 h at 37 °C under 5% CO_2. Subsequently, 10 μL MTT (5 mg/mL) was added to each well and incubated for an additional 4 h at 37 °C under 5% CO_2. After the addition of dimethyl sulfoxide (DMSO, 100 μL/well), the assay plate was allowed to stand at room temperature for 20 min. A Tecan Infinite M200 monochromator-based multi-function microplate reader was used to measure the OD570 (*Abs.* value) of each well with background subtraction at 690 nm. The following formula was used to calculate the viability of cell growth:

$$\text{cell viability}(\%) = (\text{mean of } Abs. \text{ value of treatment group} / \text{mean of } Abs. \text{ value of control}) \times 100\%.$$

2.6. Transmission electron microscopy of cells

KB cells were incubated with 200 μg/mL $Gd(OH)_3$ nanorods in a serum-free medium for 4 h at 37 °C under 5% CO_2 and washed with phosphate buffer solution (PBS) to remove excess of the $Gd(OH)_3$ nanorods. Then cells were fixed in 0.25% glutaraldehyde in PBS and postfixed in 1% osmium tetraoxide, dehydrated in ascending concentrations of ethanol and embedded in Epon 812. Ultrathin sections prepared with a LKB-1 Ultracut were lightly stained with 1% uranyl acetate and lead citrate and were observed with Philips CM120 electron microscope.

2.7. SPECT imaging in vivo of the mice injected with $^{153}Sm^{3+}$ doped $Gd(OH)_3$ nanorods

For whole-body study, a Kunming mouse which was intravenously injected with ^{153}Sm doped $Gd(OH)_3$ nanorods (20 mg/kg, ~4 mCi) was detected by nanoSPECT plus at 1, 9, 16, 51, 77 and 98 h after injection.

2.8. Analysis of the biodistribution ex vivo of $Gd(OH)_3$ nanorods

For biodistribution studies, the mice were injected with ^{153}Sm doped $Gd(OH)_3$ (2 mg/kg, ~0.4 mCi). The major organs were collected and weighed at 1, 3, 5, 24, 48, 72, 96 and 120 h post-injection. Radioactivity in the organs was measured using a γ-counter (WIZARD 1470, PerkinElmerWallac, USA) and calibrated against a known aliquot of the injection. Values are presented as mean standard deviation for three mice per group.

2.9. In vivo toxicity studies

Four weeks old Kunming mice were purchased from the Second Military Medical University (Shanghai, China). Animal procedures were in agreement with the guidelines of the Institutional Animal Care and Use Committee. The $Gd(OH)_3$ nanorods at a total dose of 100 mg/kg were injected into Kunming mice ($n = 3$) *via* the tail vein and this group of mice was test as the experimental group. Kunming mice ($n = 3$) with no injection of the $Gd(OH)_3$ nanorods were selected as the control group. The body weights of the mice in both groups were recorded for 150 days. Blood samples and tissues were harvested from mice injected with the $Gd(OH)_3$ nanorods (100 mg/kg) 30 and 150 days post-injection and from mice receiving no injection. Blood was collected from heart of the mouse quickly after it was anaesthetized. Six important hepatic indicators (alanine aminotransferase (ALT), aspartate aminotransferase (AST), Glutamyl transpeptidase (GGT), globulin (GLO), total bilirubin (TBIL) and total bile acid (TBA)), and three indicators for kidney functions (creatinine (CRE), uric acid (UA) and urea (UREA)) were measured. Upon completion of the blood collection, the mice were sacrificed. The liver, spleen, heart, lung, and kidney were removed, and fixed in paraformaldehyde, embedded in paraffin, sectioned, and stained with hematoxylin and eosin. The histological sections were observed under an optical microscope.

3. Results and discussion

3.1. Synthesis and characterization of the $Gd(OH)_3$ nanorods

The crystallinity of the $Gd(OH)_3$ samples was investigated by XRD analysis (Fig. 1a). The peak positions and intensities of the products correlate well with those calculated for the hexagonal

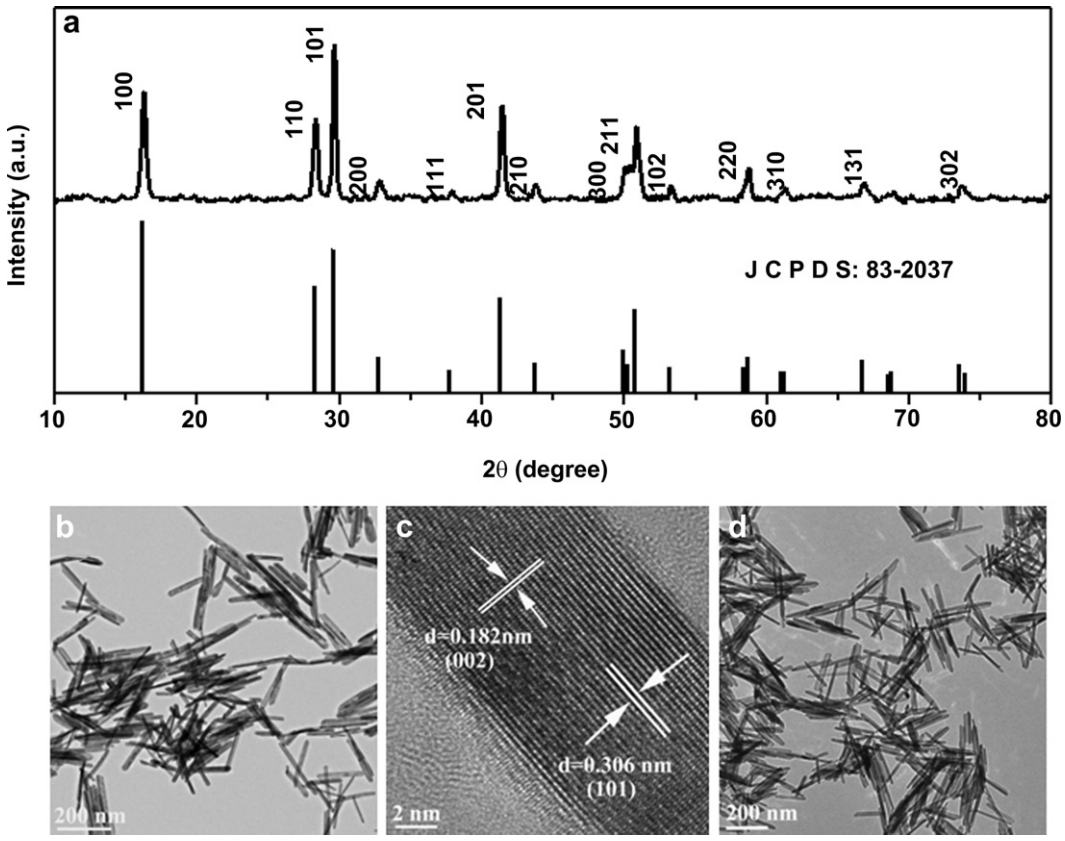

Fig. 1. (a) XRD pattern of the obtained $Gd(OH)_3$ nanorods and the standard pattern of hexagonal (JCPDS card 83-3037) phase of $Gd(OH)_3$. (b) TEM and (c) HRTEM images of the $Gd(OH)_3$ nanorods. (d) TEM images of the ^{153}Sm-doped $Gd(OH)_3$ nanorods.

phase of $Gd(OH)_3$ (JCPDS 83-2037). The TEM image (Fig. 1b) shows the as-synthesized products are nanorods with a length of 200 nm and width of 10 nm. The lattice fringes in the high-resolution TEM (HRTEM) image were indexed as the (101) and (002) planes of hexagonal $Gd(OH)_3$, confirmed by the interplanar spacing of 0.306 nm and 0.182 nm (Fig. 1c). The Fourier transform infrared (FTIR) spectrum of the $Gd(OH)_3$ samples is shown in Fig. S1. The bands below 708 cm^{-1}, assigned to Gd-O vibrational modes, and the sharp band at 3616 cm^{-1}, provide evidence of a localized OH group in $Gd(OH)_3$. The multipeak bands at approximately 2927 and 2857 cm^{-1} can be assigned to the stretching vibrations of CH_2 and the peaks at 1383 cm^{-1} and 1052 cm^{-1} are attributed to the CH_3 bending bands and N-C stretching bands, respectively, indicating the existence of triethylamine absorbed on the surface of the nanorods. In order to investigate the biodistribution of $Gd(OH)_3$ nanorods *in vivo* by SPECT imaging, the nanorods were labeled with radioactive ^{153}Sm ($E_\gamma = 103$ keV) by doping $^{153}Sm^{3+}$ ions into the

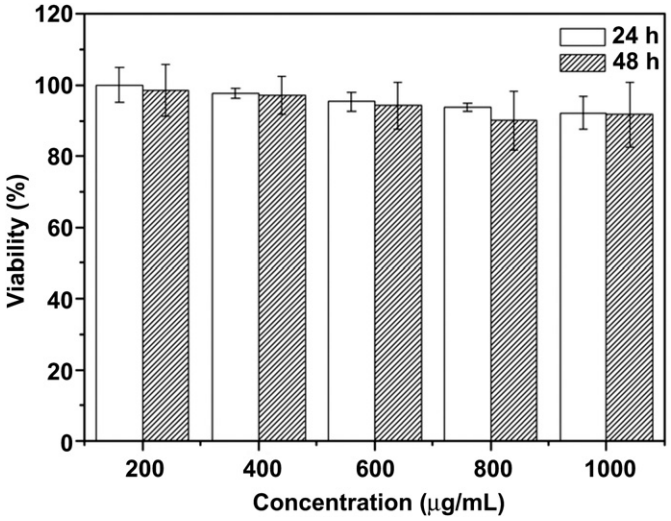

Fig. 2. Cell viability estimated by MTT assay after incubated with 200–1000 μg/mL $Gd(OH)_3$ nanorods at 37 °C for 24 h and 48 h.

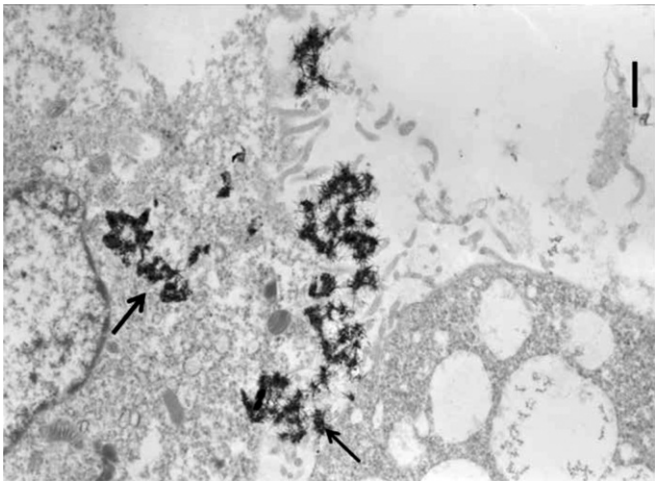

Fig. 3. TEM micrograph of KB cells incubated with 200 μg/mL $Gd(OH)_3$ nanorods for 4 h at 37 °C under 5% CO_2 (scale bar: 1 μm).

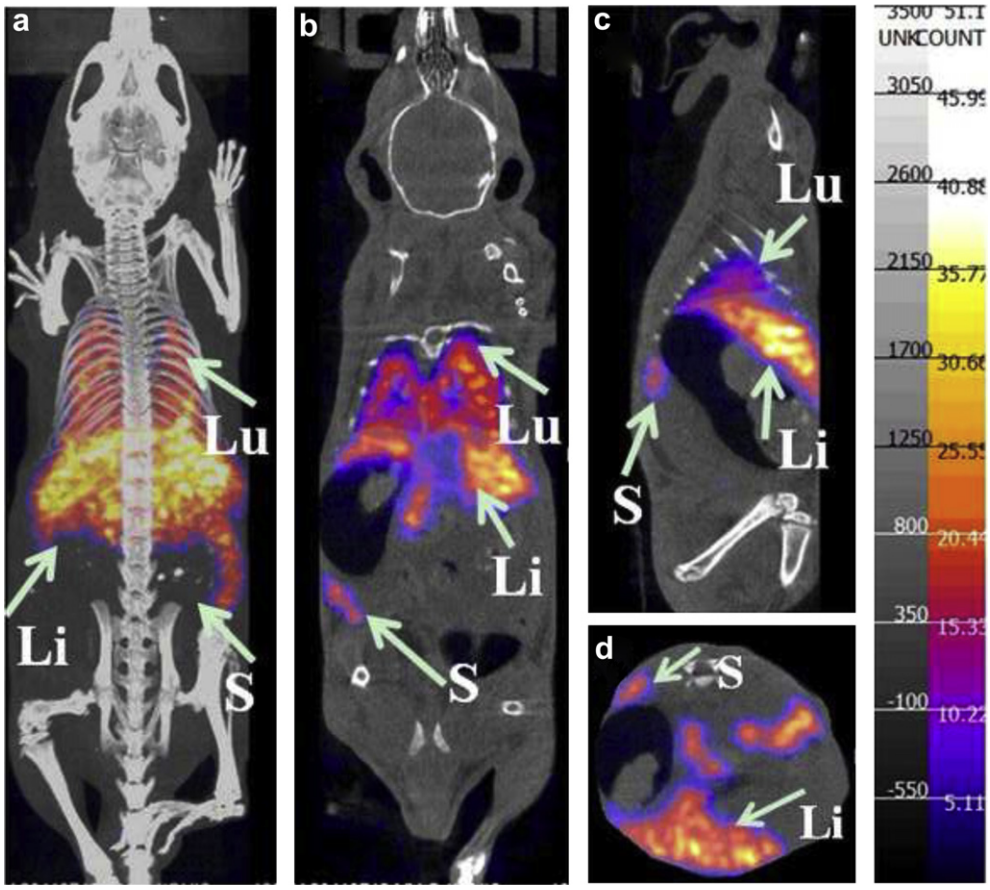

Fig. 4. *In vivo* SPECT/CT images of the mouse acquired 1 h after intravenous injection of ^{153}Sm doped $Gd(OH)_3$ nanorods. (a) whole-body three-dimensional projection, (b) coronal, (c) sagittal and (d) transversal images are shown respectively. The arrows inset point to the lung (Lu), liver (Li) and spleen (S).

$Gd(OH)_3$ nanocrystals. As $^{153}Sm^{3+}$ has a similar atomic radius and chemical characteristics to Gd^{3+}, it can be easily incorporated into the $Gd(OH)_3$ nanorods. As shown in Fig. 1d, no significant change in the shape of the $Gd(OH)_3$ nanorods has been observed before and after doping with a few radioactive $^{153}Sm^{3+}$ ions.

3.2. Cytotoxcity of the Gd $(OH)_3$ nanorods

The cytotoxicity of the $Gd(OH)_3$ nanorods were then tested by an MTT assay using KB cells as model. No obvious differences of the cell viability were observed in absence or presence of 200–1000 μg/mL $Gd(OH)_3$ nanorods, as shown in Fig. 2. After incubation with the $Gd(OH)_3$ nanorods for 24 h, the cellular viabilities were estimated to be greater than 90%. The cell viability remained >85%, even after 48 h of incubation with $Gd(OH)_3$ nanorods at a concentration as high as 1000 μg/mL. These results demonstrated that the $Gd(OH)_3$ nanorods have low cytotoxicity.

3.3. TEM image of the cells incubated with the Gd$(OH)_3$ nanorods

The internalization of the $Gd(OH)_3$ nanorods by KB cells was studied by TEM. In an electron micrograph of the cells, a large

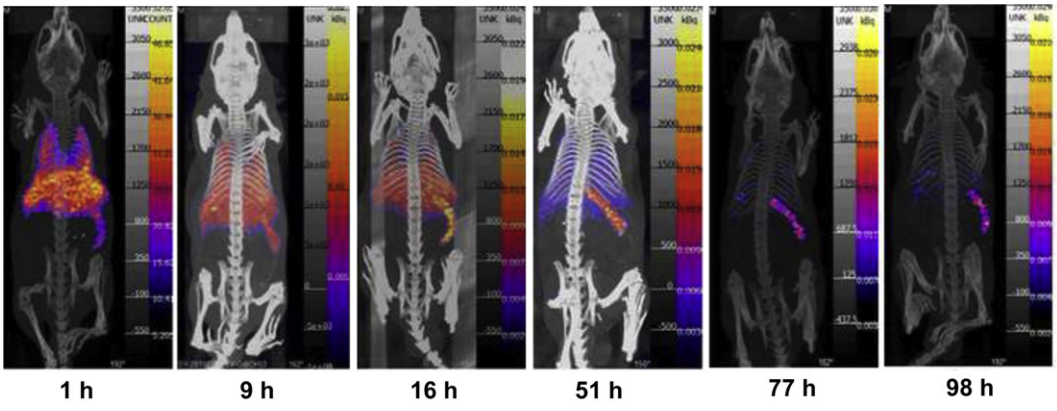

Fig. 5. SPECT/CT imagings of the mouse at different time points post-injection of ^{153}Sm-doped $Gd(OH)_3$ nanorods.

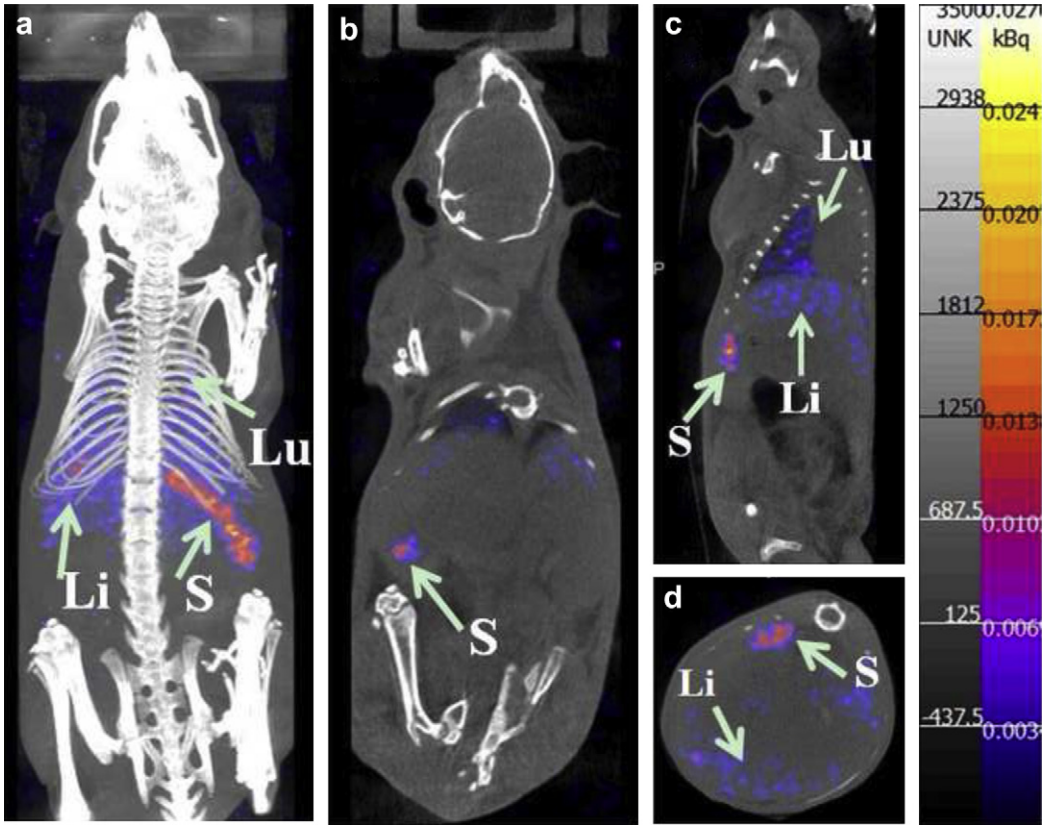

Fig. 6. *In vivo* SPECT/CT images of the mouse acquired 77 h after intravenous injection of ^{153}Sm doped $Gd(OH)_3$ nanorods. (a) whole-body three-dimensional projection, (b) coronal, (c) sagittal and (d) transversal images are shown respectively. The arrows inset point to the lung (Lu), liver (Li) and spleen (S).

number of $Gd(OH)_3$ nanorods were observed in the vesicles indicating that the $Gd(OH)_3$ nanorods were internalized into the cells (Fig. 3).

3.4. *In vivo SPECT imaging of the mice injected with ^{153}Sm-doped $Gd(OH)_3$ nanorods*

Firstly, we investigated the radiotracer release of the ^{153}Sm-doped $Gd(OH)_3$ nanorods in fetal bovine serum (FBS) buffer solution to test the labeling stability. After incubation in FBS for 24 h, all of the ^{153}Sm-doped nanorods maintained >99% labeling stability, and no free ^{153}Sm signals in the upper solutions were detected by radioactivity meter.

Next, SPECT imaging *in vivo* using the $^{153}Sm^{3+}$-doped $Gd(OH)_3$ nanorods was investigated. For these studies, a Kunming mouse was injected with ^{153}Sm-doped $Gd(OH)_3$ nanorods (20 mg/kg, ~4 mCi) through the tail vein. As shown in Fig. 4, no obvious signal was detected in the bone or bladder. As free $^{153}Sm^{3+}$ ions are mainly concentrated in the bone and excreted in the urine, this result indicated that very few free $^{153}Sm^{3+}$ ions were dissociated from the $Gd(OH)_3$ nanorods in the body. Radioactivity signals were detected predominantly in the liver, spleen and lung after the intravenous injection of ^{153}Sm-doped $Gd(OH)_3$ nanorods. No significant uptake was observed in other organs. Early accumulation in the liver and spleen is expected to be related to the clearance of nanoparticles from the blood by the mononuclear phagocytic system [48], while accumulation of nanorods in the lung is proposed as a result from their agglomeration caused by the adsorption of plasma proteins [49].

As time progressed, the signals from the liver, lung and spleen changed dramatically. As shown in Fig. 5, the uptake in the liver, spleen and lung increased during the first 9 h, reflecting the clearance of the nanorods from the bloodstream. The uptake in the spleen continued to increase up to 16 h, while the signals in the lung and liver decreased slightly. After 16 h, all of the signals in the organs decreased. After 77 h post-injection, the radioactivity signals can be found only in the spleen, and this signal maintained even after 98 h post-injection (Fig. 6). This result revealed that the excretion rate from the liver and lung is quicker than in the spleen,

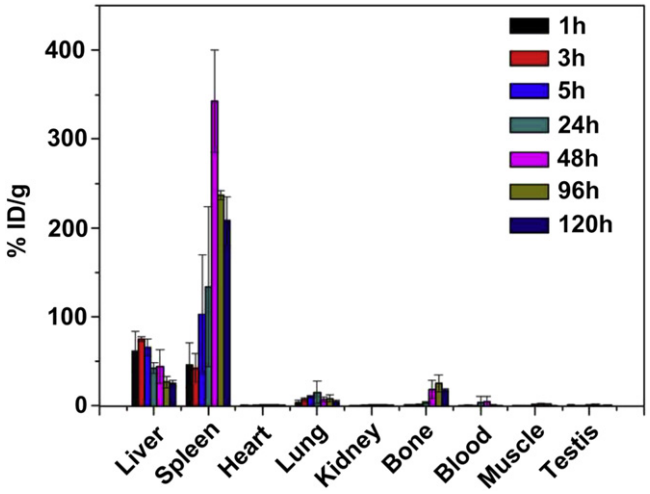

Fig. 7. *Ex vivo* distribution of ^{153}Sm doped nanorods at different time post-injection. These data were obtained by *ex vivo* distribution experiments using γ-counter and provided as mean ± SD of three independent experiments.

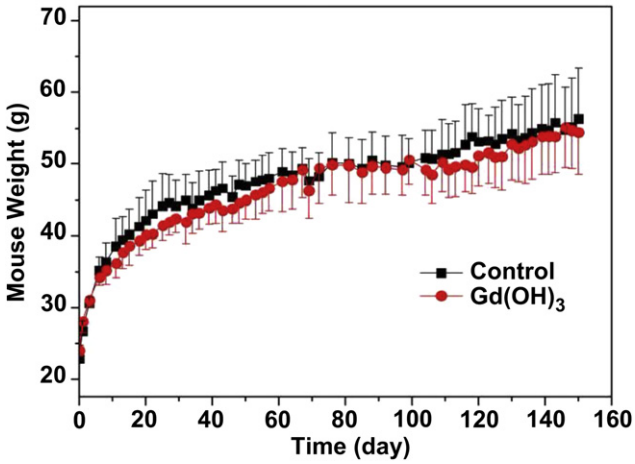

Fig. 8. Change in the body-weight of the mice injected with the $Gd(OH)_3$ nanorods ($n = 3$, dose = 100 mg/kg) and without injection ($n = 3$, Control).

which is partially due to that the spleen is the largest organ of the immune system. As a conclusion, we can see that most of such $Gd(OH)_3$ nanorods are excreted by the body quite quickly (within 51 h); afterward, excretion slowed down (77 h later).

To further understand the excretion pathway of the nanorods in the body, we investigated the quantification of the $^{153}Sm^{3+}$ signals in some other organs using the γ-counter. The total amount of materials was calculated from the radioactivity of the samples and calibrated to eliminate the influence from the decay of ^{153}Sm according to a single exponential decay model. Because the detection limits of the γ-counter are much lower than that of the nanoSPECT plus, the amount of ^{153}Sm-$Gd(OH)_3$ injected into the mice for γ-counter experiments was decreased by a factor of 10 (2 mg/kg, ~0.4 mCi) compared to that for SPECT imaging. After the mice were injected with ^{153}Sm-doped nanorods through the tail vein, various organs and tissues were collected at 1, 3, 5, 24, 48, 96 and 120 h post-injection for *ex vivo* studies. As shown in Fig. 7, the *ex vivo* determined distribution of $^{153}Sm^{3+}$-doped nanorods confirmed that the signals originated predominantly from the liver, spleen, and lung that is consistent with the SPECT images (Fig. 5). Blood analysis at 1 h detected no signals from the ^{153}Sm-doped $Gd(OH)_3$, confirming their rapid clearance from the circulating blood. Early accumulation in the liver and spleen is expected and is related to the clearance of nanorods from the blood by the cells of the mononuclear phagocytic system. Within 48 h, uptake by the spleen increased, while uptake by the liver decreased. At 48 h, a much larger uptake by the spleen versus the liver was observed, which is partially due to the spleen being the largest organ of the immune system. Then, the signals in the spleen decreased, which was consistent with the excretion of the nanorods. Interestingly, the signals in the bone increased at 48 h, which is due to partial decomposition of the nanorods in the mice, and $^{153}Sm^{3+}$ released from the $Gd(OH)_3$ nanorods was captured by the bone. It can be deduced that, after endocytosis by the cells, the nanorods are decomposed in the lysosomes where the pH value is about 4.5. Hence, $Gd(OH)_3$ nanorods can be broken down *in vivo* and excreted out from the body gradually. In particular, the biodistribution results (mainly in the liver, spleen and lung) from the lower injected amount were similar with the higher injected amount used in the SPECT imaging, whereas the metabolism and excretion of the $Gd(OH)_3$ nanorods were little different from the higher injected amount. This is partly due to the errors caused by the radioactive decay of ^{153}Sm during the SPECT imaging and partly due to the possible different metabolic pathways of the $Gd(OH)_3$ nanorods while various injected amounts were applied.

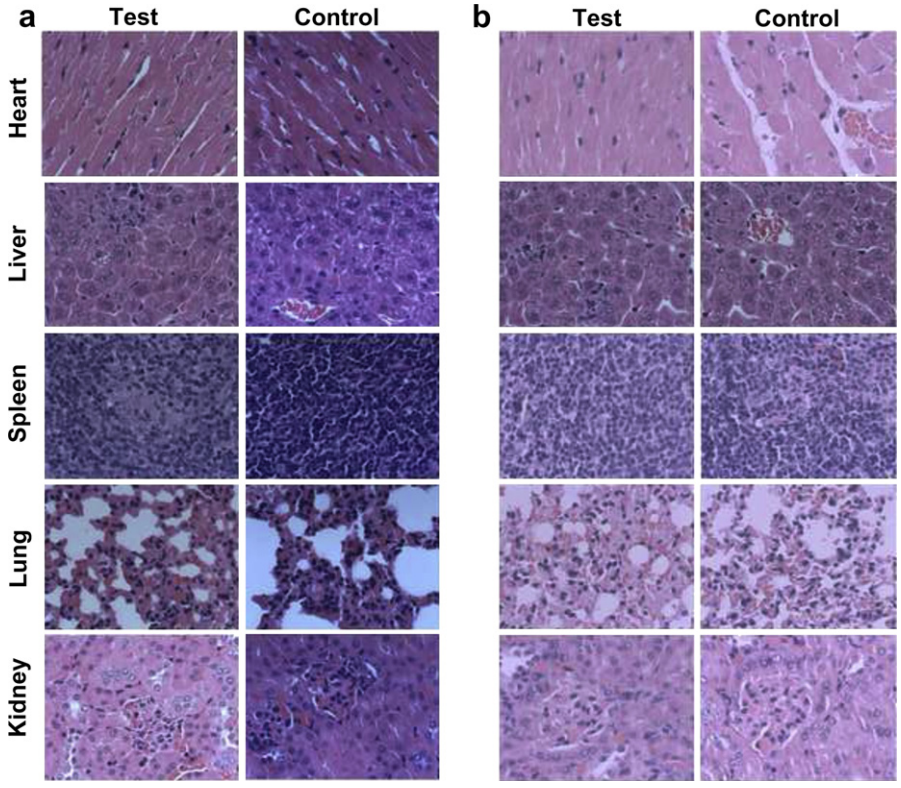

Fig. 9. H&E-stained tissue sections from mice injected with the $Gd(OH)_3$ nanorods for 30 days (a) and 150 days (b) post-injection and mice receiving no injection (Control).

3.5. Body weight measurements

Fluctuation in body weight is a useful indicator for studying the toxicity effects of the $Gd(OH)_3$ nanorods. Herein, the mice were injected with and without 100 mg/kg $Gd(OH)_3$ nanorods, which was 5 times the amount used for the SPECT imaging and 10 times the amounts used for MR imaging reported in the work of Yuan et al. [38]. Then, the body weights of the mice were recorded for 150 days and the results are shown in Fig. 8. Over a period of 7 days, the body weights of the mice injected with the $Gd(OH)_3$ nanorods increased quickly in a pattern similar to that of the control mice with no $Gd(OH)_3$ injection; during the period from day 7 to day 50, small weight differences between the two groups were observed. After 60 days, the body weights of the test group mice were approximating those of the control group mice, showing that the $Gd(OH)_3$ nanorods had no side effects on the mice from then on.

3.6. Histology and hematology results

Based on the biodistribution and excretion results, the $Gd(OH)_3$ nanorods mainly accumulated in the liver, spleen and lung, then gradually dissociated within the cells and were excreted out of the body. As a result, it is important to use the histological assessment of the tissues to determine whether or not the $Gd(OH)_3$ nanorods can cause tissue damage, inflammation or lesions due to toxic exposure. Analysis was performed on the tissues obtained from the harvested organs (heart, liver, spleen, lung, and kidney) to assess for signs of potential toxicity. As seen in Fig. 9a, the structures of the organs from the exposed mice were normal; hardly any difference was observed from those of the control group. Cardiac muscle tissue in the heart samples showed no hydropic degeneration. Hepatocytes in the liver samples appeared normal, and there were no inflammatory infiltrates. No pulmonary fibrosis was observed in the lung samples. The glomerulus structure could be distinguished easily in the kidney samples. No necrosis was found in any of the groups. However, the spleen was slightly affected by the injection of the $Gd(OH)_3$ nanorods; there was slight hyperplasia in the periarteriolar lymphoid sheath (PALS) of the white pulp, which may be caused by a nanotoxicity effect of the $Gd(OH)_3$ nanorods. This phenomenon has previously been observed in other nanoparticle-treated spleen tissues [37]. The histology and hematology results for the 150 days post-injection also showed no necrosis in the heart, liver, lung or kidney (Fig. 9b), and the spleen was back to normal as the hyperplasia in the periarteriolar lymphoid sheath (PALS) of the white pulp disappeared. The results above demonstrated the low toxicity of $Gd(OH)_3$ nanorods at exposure times as long as 150 days. Moreover, the side effects were bearable and the mice finally recovered.

Established serological tests, especially those for potential hepatic injury, spleen injury and kidney functions, were used to evaluate more quantitatively the influence of the $Gd(OH)_3$ nanorods on the exposed mice. As shown in Fig. 10a, the six important hepatic indicators, which are total bilirubin (TBIL), globulin (GLO), alanine aminotransferase (ALT), aspartate aminotransferase (AST), glutamyl transpeptidase (GGT), and total bile acid (TBA), were at similar levels for the mice exposed to the $Gd(OH)_3$ nanorods as for the control mice. The three indicators for kidney functions, uric acid (UA), urea (UREA) and creatinine (CRE), were also similar for the two groups of mice (Fig. 10a). These results suggest no significant toxicity of $Gd(OH)_3$ nanorods in mice at short exposure times (up to 30 days). All the indicators in the established serum biochemistry assays also showed no toxicity at long exposure times, even up to 150 days (Fig. 10b) Therefore, based on the results above, the $Gd(OH)_3$ nanorods are safe for use *in vivo*.

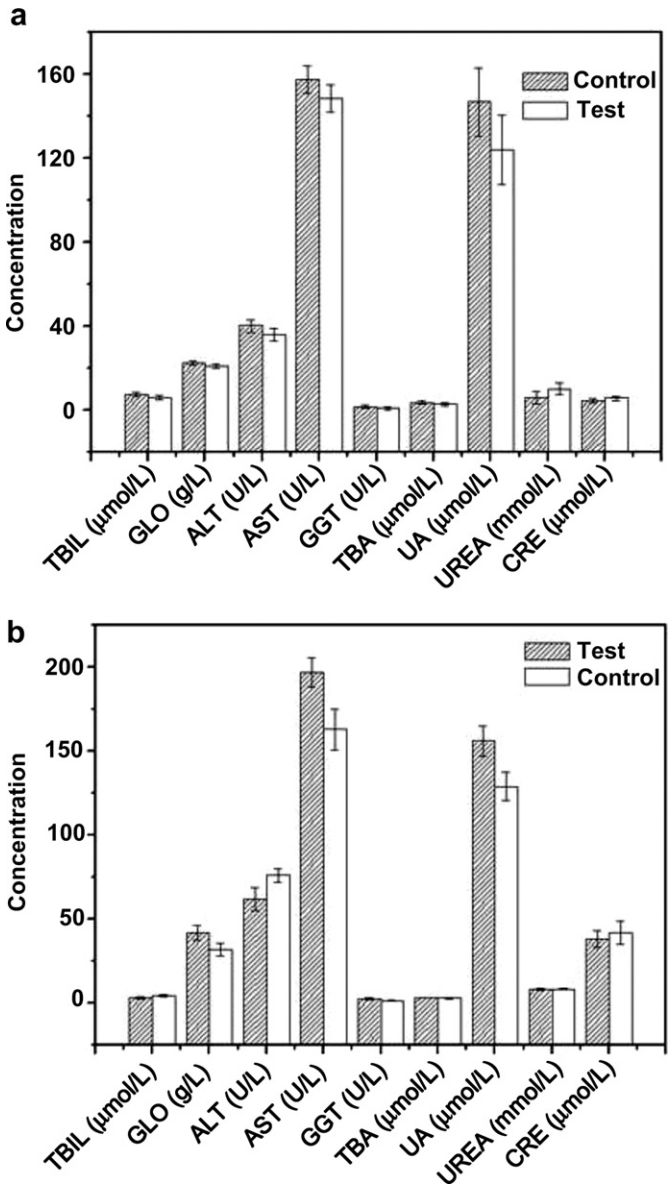

Fig. 10. Serological test results obtained from mice injected with $Gd(OH)_3$ for 30 days (a) and 150 days (b) post-injection ($n = 3$, dose = 100 mg/kg, Test) and mice receiving no injection ($n = 3$, Control).

4. Conclusion

We reported the long-term *in vivo* biodistribution and toxicity studies of the $Gd(OH)_3$ nanorods. *In vitro* cytotoxicity results showed that the $Gd(OH)_3$ nanorods have no significant effects on the proliferation of KB cells, and the cellular viabilities were estimated to be greater than 85% after 48 h incubation with the $Gd(OH)_3$ nanorods ($\leq$1 mg/mL). Biodistribution results by both *in vivo* SPECT imaging and λ-counter experiments showed that most of the $Gd(OH)_3$ nanorods were cleared from the bodies of mice quickly. However, excretion from the spleen was slower than from other organs. Furthermore, *in vivo* toxicity studies indicated that mice intravenously injected with up to 100 mg/kg of $Gd(OH)_3$ (5 times the injected amount used in SPECT imaging) survived without any evident (observational, histological, hematological or biochemical) toxic effects at exposure times as long as 150 days. These studies provide preliminary validation for the use of $Gd(OH)_3$ nanorods for long-term *in vivo* imaging.

Acknowledgments

This work was financially supported by NSFC (20825101 and 20775017), the State Key Basic Research Program of China (2011AA03A407 and 2012CB932403), Shanghai Sci. Tech. Comm. (1052nm03400), IRT0911, SLADP (B108) and the CAS/SAFEA International Partnership Program for Creative Research Teams. The authors also acknowledge Dr. Jing Zhou and Qian Liu for discussion.

Appendix A. Supplementary data

Supplementary data related to this article can be found at http://dx.doi.org/10.1016/j.biomaterials.2012.09.075.

References

[1] Sarakovskis A, Voss M, Doke G, Grube J, Springis J. Novel synthesis of upconversion phosphor based on rare-earth doped $NaLaF_4$. IOP Conf Ser: Mater Sci Eng 2011;23:012003.
[2] Wang F, Liu XG. Recent advances in the chemistry of lanthanide-doped upconversion nanocrystals. Chem Soc Rev 2009;38:976–89.
[3] Bogdan N, Vetrone F, Ozin GA, Capobianco JA. Synthesis of ligand-free colloidally stable water dispersible brightly luminescent lanthanide-doped upconverting nanoparticles. Nano Lett 2011;11:835–40.
[4] Wang LY, Yan RX, Hao ZY, Wang L, Zeng JH, Bao H, et al. Fluorescence resonant energy transfer biosensor based on upconversion-luminescent nanoparticles. Angew Chem Int Ed 2005;44:6054–7.
[5] Yang PP, Quan ZW, Hou ZY, Li CX, Kang XJ, Cheng ZY, et al. A magnetic, luminescent and mesoporous core-shell structured composite material as drug carrier. Biomaterials 2009;30:4786–95.
[6] Achatz DE, Meier RJ, Fischer LH, Wolfbeis OS. Luminescent sensing of oxygen using a quenchable probe and upconverting nanoparticles. Angew Chem Int Ed 2011;50:260–3.
[7] Shen J, Sun LD, Zhu JD, Wei LH, Sun HF, Yan CH. Biocompatible bright YVO_4: Eu nanoparticles as versatile optical bioprobes. Adv Funct Mater 2010;20:3708–14.
[8] Jiang S, Zhang Y. Upconversion nanoparticle-based FRET system for study of siRNA in live cells. Langmuir 2010;26:6689–94.
[9] Boyer JC, Cuccia LA, Capobianco JA. Synthesis of colloidal upconverting $NaYF_4$: Er^{3+}/Yb3+ and Tm^{3+}/Yb^{3+} monodisperse nanocrystals. Nano Lett 2007;7:847–52.
[10] Naccache R, Vetrone F, Mahalingam V, Cuccia LA, Capobianco JA. Controlled synthesis and water dispersibility of hexagonal phase $NaGdF_4$:Ho^{3+}/Yb^{3+} nanoparticles. Chem Mater 2009;21:717–23.
[11] Cao TY, Yang Y, Gao Y, Zhou J, Li ZQ, Li FY. High-quality water-soluble and surface-functionalized upconversion nanocrystals as luminescent probes for bioimaging. Biomaterials 2011;32:2959–68.
[12] Wang GF, Peng Q, Li YD. Upconversion luminescence of monodisperse CaF_2: Yb^{3+}/Er^{3+} nanocrystals. J Am Chem Soc 2009;131:14200–1.
[13] Zhang CM, Ma PA, Li CX, Li GG, Huang SS, Yang DM, et al. Controllable and white upconversion luminescence in $BaYF_5$:Ln^{3+} (Ln = Yb, Er, Tm) nanocrystals. J Mater Chem 2011;21:717–23.
[14] Mai HX, Zhang YW, Si R, Yan ZG, Sun LD, You LP, et al. High-quality sodium rare-earth fluoride nanocrystals: controlled synthesis and optical properties. J Am Chem Soc 2006;128:6426–36.
[15] Niu N, Yang P, He F, Zhang X, Gai S, Li C, et al. Tunable multicolor and bright white emission of one-dimensional $NaLuF_4$:Yb^{3+}, Ln^{3+} (Ln = Er, Tm, Ho, Er/Tm, Tm/Ho) microstructures. J Mater Chem 2012;22:10889–99.
[16] Yu MX, Li FY, Chen ZG, Hu H, Zhan C, Yang H, et al. Laser scanning upconversion luminescence microscopy for imaging cells labeled with rare-earth nanophosphors. Anal Chem 2009;81:930–5.
[17] Xiong LQ, Chen ZG, Tian QW, Cao TY, Xu CJ, Li FY. High contrast upconversion luminescence targeted imaging in vivo using peptide-labeled nanophosphors. Anal Chem 2009;81:8687–94.
[18] Hu H, Xiong LQ, Zhou J, Li FY, Cao TY, Huang CH. Multimodal-luminescence core-shell nanocomposites for targeted imaging of tumor cells. Chem Eur J 2009;15:3577–84.
[19] Wang GF, Li Y, Jiang BJ, Pan K, Fan NY, Feng QM, et al. In situ synthesis and photoluminescence of Eu^{3+} doped $Y(OH)_3$@beta-$NaYF_4$ core-shell nanotubes. Chem Commun 2011;47:8019–21.
[20] Steiner MS, Duerkop A, Wolfbeis OS. Optical methods for sensing glucose. Chem Soc Rev 2011;40:4805–39.
[21] Nyk M, Kumar R, Ohulchanskyy TY, Bergey EJ, Prasad PN. High contrast in vitro and in vivo photoluminescence bioimaging using near infrared to near infrared up-conversion in Tm^{3+} and Yb^{3+} doped fluoride nanophosphors. Nano Lett 2008;8:3834–8.
[22] Chatteriee DK, Rufalhah AJ, Zhang Y. Upconversion fluorescence imaging of cells and small animals using lanthanide doped nanocrystals. Biomaterials 2008;29:937–43.
[23] Idris NM, Li ZQ, Ye L, Sim EKW, Mahendran R, Ho PCL, et al. Tracking transplanted cells in live animal using upconversion fluorescent nanoparticles. Biomaterials 2009;30:5104–13.
[24] Hu H, Bai Y. Upconversion white luminescence of TeO_2: $Tm^{3+}/Er^{3+}/Yb^{3+}$ nanoparticles. J Alloys Compd 2012;527:25–9.
[25] Zhou J, Sun Y, Du XX, Xiong LQ, Hu H, Li FY. Dual-modality in vivo imaging using rare-earth nanocrystals with near-infrared to near-infrared (NIR-to-NIR) upconversion luminescence and magnetic resonance properties. Biomaterials 2010;31:3287–95.
[26] Park YI, Kim JH, Lee KT, Jeon K-S, Na HB, Yu JH, et al. Nonblinking and nonbleaching upconverting nanoparticles as an optical imaging nanoprobe and T_1 magnetic resonance imaging contrast agent. Adv Mater 2009;21:4467–71.
[27] Kumar R, Nyk M, Ohulchanskyy TY, Flask CA, Prasad PN. Combined optical and MR bioimaging using rare earth ion doped $NaYF_4$ nanocrystals. Adv Funct Mater 2009;19:853–9.
[28] Mack J, Kobayashi N. Low symmetry phthalocyanines and their analogues. Chem Rev 2010;111:281–321.
[29] Sun Y, Yu MX, Liang S, Zhang YJ, Li CG, Mou TT, et al. Fluorine-18 labeled rare-earth nanoparticles for positron emission tomography (PET) imaging of sentinel lymph node. Biomaterials 2011;32:2999–3007.
[30] Zhou J, Yu MX, Sun Y, Zhang XZ, Zhu XJ, Wu ZH, et al. Fluorine-18-labeled $Gd^{3+}/Yb^{3+}/Er^{3+}$ co-doped $NaYF_4$ nanophosphors for multimodality PET/MR/UCL imaging. Biomaterials 2011;32:1148–56.
[31] Liu Q, Sun Y, Li CG, Zhou J, Li CY, Yang TS, et al. ^{18}F-Labeled magnetic-upconversion nanophosphors via rare-earth cation-assisted ligand assembly. ACS Nano 2011;5:3146–57.
[32] Xing H, Bu W, Ren Q, Zheng X, Li M, Zhang S, et al. A $NaYbF_4$: Tm^{3+} nanoprobe for CT and NIR-to-NIR fluorescent bimodal imaging. Biomaterials 2012;33:5384–93.
[33] Zhu XJ, Zhou J, Chen M, Shi M, Feng W, Li FY. Core–shell Fe_3O_4@$NaLuF_4$:Yb, Er/Tm nanostructure for MRI, CT and upconversion luminescence tri-modality imaging. Biomaterials 2012;33:4618–27.
[34] Xia A, Chen M, Gao Y, Wu DM, Feng W, Li FY. Gd^{3+} complex-modified $NaLuF_4$-based upconversion nanophosphors for trimodality imaging of NIR-to-NIR upconversion luminescence, X-Ray computed tomography and magnetic resonance. Biomaterials 2012;33:5394–405.
[35] Jalil RA, Zhang Y. Biocompatibility of silica coated $NaYF_4$ upconversion fluorescent nanocrystals. Biomaterials 2008;29:4122–8.
[36] Cheng L, Yang K, Shao MW, Lu XH, Liu Z. In vivo pharmacokinetics, long-term biodistribution and toxicology study of functionalized upconversion nanoparticles in mice. Nanomedicine UK 2011;6:1327–40.
[37] Xiong LQ, Yang TS, Yang Y, Xu CJ, Li FY. Long-term in vivo biodistribution imaging and toxicity of polyacrylic acid-coated upconversion nanophosphors. Biomaterials 2010;31:7078–85.
[38] Huang S, Liu J, Liu D, Yuan Q. Facile and large-scale synthesis of $Gd(OH)_3$ nanorods for MR imaging with low toxicity. New J Chem 2012;36:1335–8.
[39] Kryza D, Taleb J, Janier M, Marmuse L, Miladi I, Bonazza P, et al. Biodistribution study of nanometric hybrid gadolinium oxide particles as a multimodal SPECT/MR/Optical imaging and theragnostic agent. Bioconjug Chem 2011;22:1145–52.
[40] Park J-A, Kim JY, Kim H-K, Lee W, Lim SM, Chang Y, et al. Heteronuclear Gd-99mTc complex of DTPA-bis(histidylamide) conjugate as a bimodal MR/SPECT imaging probe. ACS Med Chem Lett 2012;3:299–302.
[41] Merkel OM, Librizzi D, Pfestroff A, Schurrat T, Behe M, Kissel T. In vivo SPECT and real-time gamma camera imaging of biodistribution and pharmacokinetics of siRNA delivery using an optimized radiolabeling and purification procedure. Bioconjug Chem 2008;20:174–82.
[42] Adam MJ, Wilbur DS. Radiohalogens for imaging and therapy. Chem Soc Rev 2005;34:153–63.
[43] Bowen ML, Orvig C. 99m-Technetium carbohydrate conjugates as potential agents in molecular imaging. Chem Commun 2008:5077–91.
[44] Niers JM, Chen JW, Lewandrowski G, Kerami M, Garanger E, Wojtkiewicz G, et al. Single reporter for targeted multimodal in vivo imaging. J Am Chem Soc 2012;134:5149–56.
[45] Pimlott SL, Sutherland A. Molecular tracers for the PET and SPECT imaging of disease. Chem Soc Rev 2011;40:149–62.
[46] Bhushan KR, Misra P, Liu F, Mathur S, Lenkinski RE, Frangioni JV. Detection of breast cancer microcalcifications using a dual-modality SPECT/NIR fluorescent probe. J Am Chem Soc 2008;130:17648–9.
[47] Brinkhuis RP, Stojanov K, Laverman P, Eilander J, Zuhorn IS, Rutjes FPJT, et al. Size dependent biodistribution and SPECT imaging of ^{111}In-labeled polymersomes. Bioconjug Chem 2012;23:958–65.
[48] Dobrovolskaia MA, Aggarwal P, Hall JB, McNeil SE. Preclinical studies to understand nanoparticle interaction with the immune system and its potential effects on nanoparticle biodistribution. Mol Pharmaceutics 2008;5:487–95.
[49] Alexis F, Pridgen E, Molnar LK, Farokhzad OC. Factors affecting the clearance and biodistribution of polymeric nanoparticles. Mol Pharmaceutics 2008;5:505–15.